JOURNAL OF PROPULSION AND POWER
Vol. 22, No. 4, July–August 2006

Design and Test of a Modular Waverider Hypersonic Intake

A. J. Matthews* and T. V. Jones†
University of Oxford, Oxford, England OX1 3PJ, United Kingdom

A study of some modular stream-traced hypersonic intakes is presented. These intakes capture a part of a known flowfield by replacing the streamlines that pass through the perimeter of a sector capture shape with solid boundary-layer-corrected surfaces. Modules are combined to form an engine with a circular external profile and with each intake module feeding a separate combustor. The intakes studied are derived from internally compressive, axisymmetric flowfields with either constant slope or constant pressure boundary conditions. The number of modules varies between three and six. Stream thrust averaging is used to determine equivalent one-dimensional flow for input to a scramjet engine cycle analysis. For a given contraction ratio, the full mass capture engine performance of the modular waverider intakes is comparable with the performance of isentropic spike intake designs when combustor skin friction is neglected. However, the low wetted area of the modular combustor design has a significant advantage when combustor skin friction is considered. A four-module waverider intake model was built using stereolithography and tested at Mach 7 in the University of Oxford gun tunnel and was shown to be self-starting in QinetiQ's High Density Tunnel at Mach 7. The stream thrust averaged properties were determined experimentally by measurement of axial force and mass capture. Schlieren photographs and surface pressure measurements are presented. Skin friction in the model isolator section was found to affect intake performance by increasing the amount of compression and reducing efficiency.

Nomenclature

A	=	area, m^2
D_∞	=	full capture diameter, m
F	=	force, N
g	=	acceleration due to gravity, m/s^2
h	=	specific enthalpy, referenced to 25°C, J/kg
I_{sp}	=	specific impulse, $F_T/\dot{m}_{H2}g$, s
M	=	Mach number
$\dot{m}$	=	mass flow rate, kg/s
N	=	number of modules
p	=	pressure, Pa
p_{02}/p_{01}	=	total pressure recovery
Q	=	heat transfer, W
R	=	gas constant, J/kg/K
Re_D	=	Reynolds number, $\rho_1 v_1 D_\infty/\mu_1$
R_{EXC}	=	cowl radius-to-initial duct height ratio for external compression (EXC) intakes
r	=	radius, m
r, ϕ, z	=	cylindrical polar coordinates (defined in Fig. 2)
T	=	temperature, K
v	=	velocity, m/s
x, y, z	=	Cartesian coordinates
η_{KE}	=	kinetic energy efficiency, $[h_{02} - h(p_1, s_2)]/(h_{01} - h_1)$
θ_{w1}	=	initial boundary slope in modular waverider baseline flowfield, deg
θ_1	=	initial cone/wedge angle for reexpansion (REX) and EXC intakes, deg
θ_2	=	final wall slope for REX and EXC intakes, deg
μ	=	dynamic viscosity, Pa · s
ρ	=	density, kg/m^3

Subscripts

add	=	preentry (additive) drag
b	=	base pressure
CD	=	cowl drag
c	=	cowl closure plane
e	=	scramjet engine exit plane
f	=	frictional force
geo	=	geometric
H2	=	hydrogen
I	=	isolator
K	=	Kantrowitz limit
LC	=	load cell
p	=	pressure force
pl	=	plenum
s	=	surface area
T	=	thrust
t	=	pitot pressure
w	=	wall
x	=	axial force, cross-sectional area
0	=	total conditions
1	=	captured flow freestream conditions
2	=	mixed to uniform conditions at intake exit
∞	=	full mass capture freestream conditions

Presented as Paper 2005-3379 at the AIAA/CIRA 13th International Space Planes and Hypersonics Systems and Technologies Conference, Capua, 16–20 May 2005; received 3 June 2005; revision received 30 December 2005; accepted for publication 30 December 2005.

*Departmental Lecturer, Department of Engineering Science, Parks Road. Member AIAA.

†D. Schultz Professor of Turbomachinery, Department of Engineering Science, Parks Road.

I. Introduction

WAVERIDER (stream-traced) intakes[1–5] are designed to capture part of a known baseline flowfield by identifying the streamlines that pass through the perimeter of a specified capture shape and replacing them with solid, boundary-layer-corrected surfaces downstream of the leading-edge shock wave. This procedure generates a mixed external–internal compression intake with a leading-edge shock wave that rests along the intake edges at the design condition. Modular waverider (MW) intakes have been designed with sector capture shapes that tessellate to form an intake with a circular external profile and with each intake module feeding a separate combustor.[1,2] These intakes alleviate the starting problem for internal compression flowfields and have swept leading edges, which are favorable for heat transfer considerations. The intakes have low cowl drag, but skin friction can be high due to large wetted areas.

A parametric study of MW intakes is presented, investigating the effect of changing the baseline flowfield and the number of

modules. Nonuniform flows delivered by the intakes are stream thrust averaged[6] (mixed out to uniform conditions using a control volume approach) to conserve the mass flow, momentum, and energy of the true flowfield, and intake performance is assessed using an engine cycle analysis.[7] The design-point performance of MW intakes are compared against isentropic-spike designs using this approach.

An MW intake model was tested in the University of Oxford gun tunnel. The stream-thrust-averaged flow delivered by the intake was determined by solving the conservation equations for the intake's captured flow control volume using measured values of axial force and mass capture. Intake self-starting ability was determined in QinetiQ's High Density Tunnel.

II. MW Intake Design

Figures 1–3 show the baseline flowfields, the MW sector capture shape dimensions, and a geometric MW intake module, respectively. Inviscid, axisymmetric, internal-compression flowfields were calculated using the method of characteristics (MOC). The boundaries were designed to hold constant pressure (CPS) or constant slope (CSS) (Fig. 1). The location and size of the Mach disk was calculated assuming that the pressure downstream of the reflected shock would not exceed normal shock pressure. The reflected shock wave was found approximately by enforcing parallel flow downstream of the Mach disk and applying the Rankine–Hugoniot shock wave equations, knowing the calculated flowfield upstream of the shock wave.

MW intakes were designed to capture the portion of the baseline flowfield within the sector capture shape shown in Fig. 2. The inviscid MW surfaces were created by identifying the streamlines in the baseline flowfield that pass through the perimeter of the sector capture shape and tracing them as they extend downstream from the leading-edge shock wave to the reflected shock. Downstream of the reflected shock wave the waverider surfaces were made parallel to the external flow.

Geometric MW intakes (Fig. 3) were created by applying an approximate local-flat-plate correction for boundary-layer displacement thickness to the inviscid MW surfaces. The momentum integral method was used, with skin friction and heat transfer calculated from a turbulent flat-plate correlation based on momentum thickness with properties evaluated at Eckert's reference temperature.[8] Constant values of 0.9 and 0.8 were assumed for the recovery factor and Reynolds analogy factor, respectively,[9] and Stollery's flat-plate values for shape factor were used.[10] The intake surface was assumed to be at uniform temperature calculated by integrating heat transfer over the compression surface and equating this to the radiation from the surface assuming an emissivity of 0.8. This method may underestimate the correct displacement thickness for the MW flowfields because they have adverse pressure gradients and regions of strong lateral inward-turning curvature. However, the use of a local-flat-plate calculation in flows with adverse pressure gradients and lateral curvature is supported by its simplicity and its reasonable agreement with experiment.[7,10]

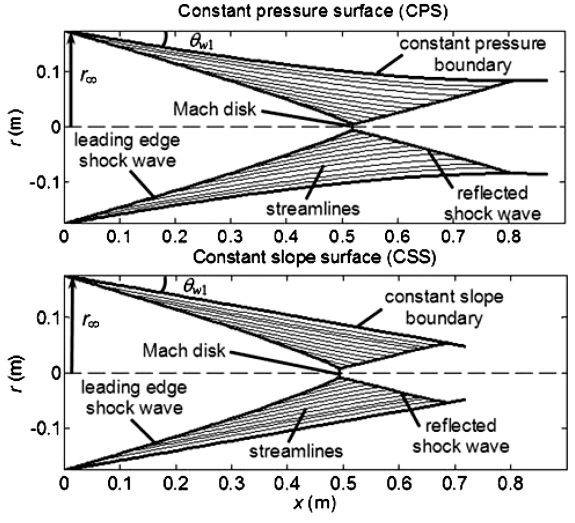

Fig. 1 MOC solutions of axisymmetric internal compression baseline flowfields, $M_1 = 7.0$ and $\theta_{w1} = 10$ deg.

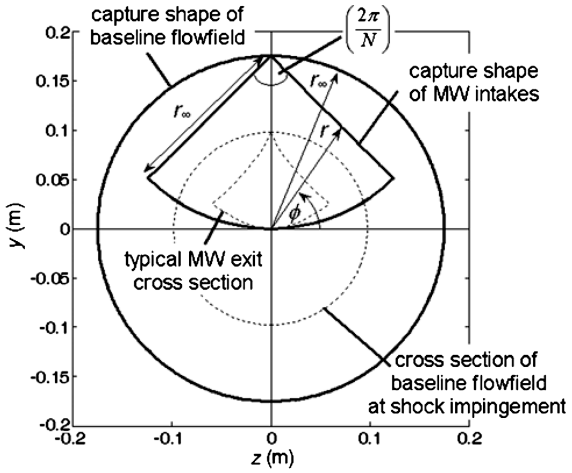

Fig. 2 Sector capture shape for MW intakes.

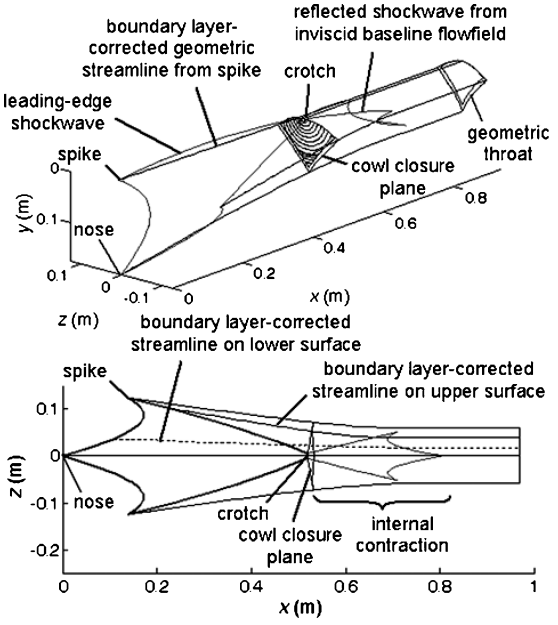

Fig. 3 CPS intake module with $N = 4$ and $\theta_{w1} = 10$ deg.

The starting characteristics of the MW intakes were estimated using the Kantrowitz and Donaldson starting criterion.[11] This assumes that at the limiting internal contraction, the subsonic flow downstream of a normal shock wave situated at the cowl closure plane accelerates to Mach 1 at the intake throat. To account for nonuniform flow, the cowl closure plane was taken to be the curved surface originating at the crotch that is at all points normal to the flow. A normal shock wave coplanar with this curved surface creates a nonuniform subsonic flow. Incremental areas of this subsonic flow were assumed to accelerate independently and one dimensionally to Mach 1, and the sum of incremental areas at Mach 1 was taken to be the limiting Kantrowitz throat. It is recognized that the boundary layer in the unstarted condition bears no resemblance to that with the design flow, and an experiment is required to really determine the maximum self-starting internal-contraction ratio.

Calculated internal contractions for CPS and CSS MW intakes are shown in Fig. 4. The Kantrowitz limit does not vary significantly with N and lies along the dotted line shown. Because the geometric internal contractions are generally greater than the Kantrowitz limit

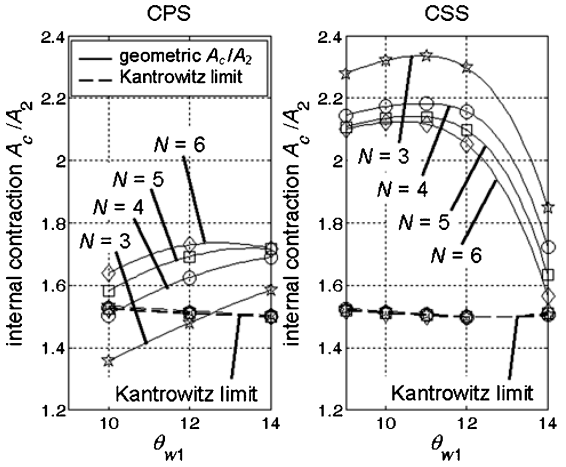

Fig. 4 Geometric internal contractions of CPS and CSS MW intakes.

it is apparent that these intakes, in particular the CSS MW intakes, may be limited by starting requirements.

III. Intake Performance

The performance of a hypersonic intake is a function of the compression performed (intake capability), the efficiency of the compression process, mass capture, and intake contribution to vehicle drag. To assess the relative performance of intake concepts, engine performance is calculated by coupling the intake to an ideal combustor and nozzle. To account for nonuniform flow at the intake exit, a one-dimensional representation that conserves the mass flow, momentum, and energy of the true flowfield is used. This is referred to as stream-thrust-averaged flow and is calculated using a control volume analysis with nonuniform intake flow entering one end of a constant-area duct and fully mixed-out uniform flow exiting the other. Mixing losses cause the entropy of the flow to increase, hence stream-thrust-averaged intake efficiencies appear low when compared to those calculated using other approaches such as mass flow averaging or area averaging. However, mixing losses are necessary in the combustor to disperse and mix the fuel with the air; by using stream-thrust-averaged flow properties as input to the combustor in an engine cycle analysis, mixing losses are attributed to the intake and an ideal combustor is assumed.

Engine exhaust velocity and pressure were calculated with the following assumptions: 1) Combustor entry flow conditions are the stream-thrust-averaged properties at the intake exit. 2) Hydrogen fuel is injected normal to the engine axis at stoichiometric conditions. 3) Combustor area is constant, or diverges such that the flow is thermally choked at the combustor exit. 4) Pressure is assumed to vary linearly with area in a diverging combustor. 5) Combustor heat loss and skin friction are zero. 6) The mixture is in chemical equilibrium within the combustor. 7) The mixture is either in equilibrium or frozen within the nozzle. 8) The nozzle exit area is fixed at $A_e/A_\infty = 2$.

Mixture properties were calculated using the NASA Lewis Chemical Equilibrium Program (CEA),[12,13] and engine performance is presented in terms of the specific impulse. Thrust coefficients are not presented because, for all cases here, $C_T = F_T/\frac{1}{2}\rho_1 v_1^2 A_e$ and $I_{sp} = F_T/\dot{m}_{H2}g$ follow the same trends because nozzle exit area, fuel mass flow rate, and the freestream dynamic pressure are fixed.

IV. Calculated MW Intake Performance

The calculated stream-thrust-averaged capability of geometric (viscous) CPS and CSS MW intakes are presented in Fig. 5. The results are for full mass capture at $M_1 = 7.0$, $Re_D = 1.57 \times 10^6$, and with $D_\infty = 0.35$ m. The capability of these intakes initially increases with θ_{w1} until the growth of the Mach disk in the baseline flowfield causes the total contractions of the stream-traced intakes to decrease by pushing the impingement point of the reflected shock farther upstream. This is seen to occur around $\theta_{w1} > 12$ deg for the CSS MW

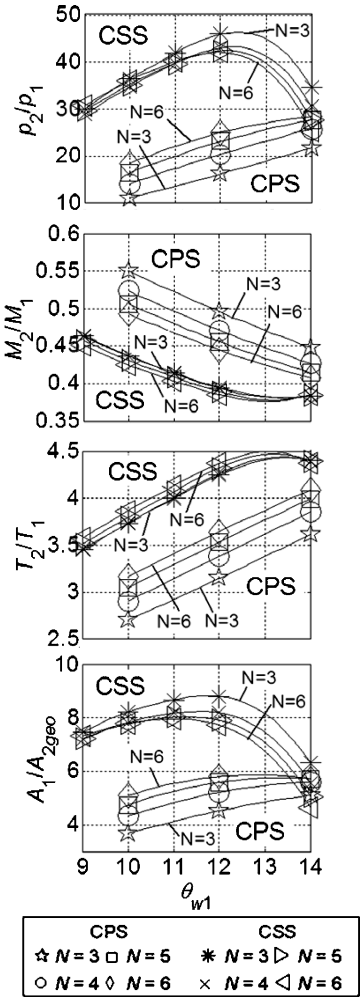

Fig. 5 MW capability parameters.

intakes and is expected to occur at higher angles for the CPS MW intakes. When N is varied, different streamlines are selected, which changes the intake geometry and the boundary-layer edge properties, hence, the stream-thrust-averaged flows change. The capability of CPS MW intakes increases steadily with N, but for CSS MW intakes the variation with N is far less, coinciding with less variation in geometry and flow properties between adjacent streamlines. In general, the compression performed by CSS MW intakes is significantly higher than for CPS MW intakes.

Efficiency parameters are presented in Fig. 6. The dotted/dashed lines represent inviscid adiabatic intakes, and the solid lines represent geometric viscous intakes. For clarity, only the results for $N = 3$ and 6 intakes are shown; $N = 4$ and 5 intake efficiencies lie within these limits. The efficiency of CPS and CSS MW intakes decreases with θ_{w1} as wave losses increase. CSS MW intake efficiency decreases further for $\theta_{w1} > 12$ deg as the growth of the Mach disk reduces the total contraction (Fig. 5). For a given θ_{w1}, the efficiencies of CSS and CPS MW intakes are similar and show only modest variation with N. This variation is less for CPS MW intakes than CSS MW intakes because the axial force and total contraction (which have a greater variation with N for the CPS MW intakes) have conflicting effects on efficiency. Skin friction is higher in MW intakes than it is in the baseline flowfields as a consequence of having more module wetted area; its effect is more apparent in the longer intakes with lower θ_{w1}. There is also a loss of efficiency associated with reducing the geometric contraction ratio when applying a boundary-layer correction to account for the physical displacement of the inviscid flowfield.

At low θ_{w1} where the effects of the Mach disk on total contraction are small, Figs. 5 and 6 show the general trend for hypersonic

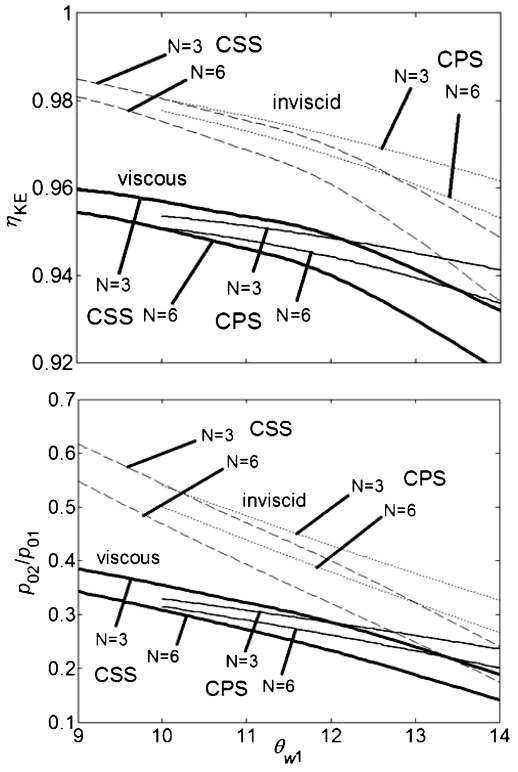

Fig. 6 MW efficiency parameters.

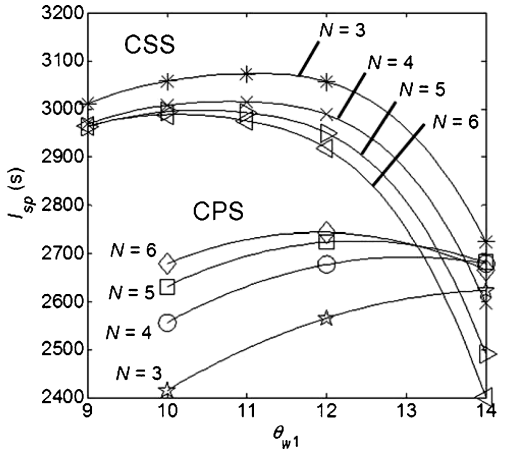

Fig. 7 Engine performance of MW intakes.

intakes that an increase of capability is usually accompanied by an associated decrease of efficiency. An engine cycle analysis is, therefore, necessary to determine the true effect of intake design changes. Engine cycle performance is presented in Fig. 7 in terms of the specific impulse. For clarity, only the curves for equilibrium nozzle flow are shown; the same trends are apparent but at lower I_{sp} if frozen flow is assumed. For a given number of modules it is apparent that, for all intakes here, an optimum θ_{w1} exists, where the effects of intake capability and efficiency on engine performance are balanced. For CPS MW intakes, engine performance increases with N but this trend is reversed for CSS MW intakes, indicating that I_{sp} is strongly influenced by total contraction (Fig. 5). Specific impulse is higher for CSS MW due to their higher contractions and capability; however, these intakes also have high internal contractions and may suffer from starting difficulties (Fig. 4).

Figure 8 shows the variations of specific impulse at full mass capture as a function of total contraction ratio for given values of N. (CSS MW intakes with $\theta_{w1} = 14$ deg are not shown.) The optimum I_{sp} for each curve coincides with the maximum total contraction,

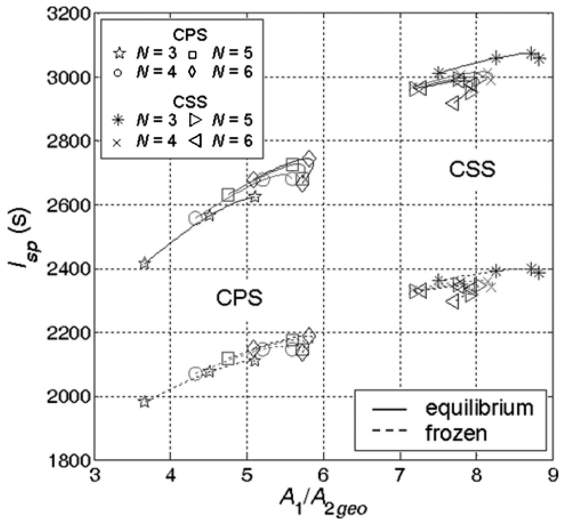

Fig. 8 Engine performance as function of intake type, number of modules, and total contraction.

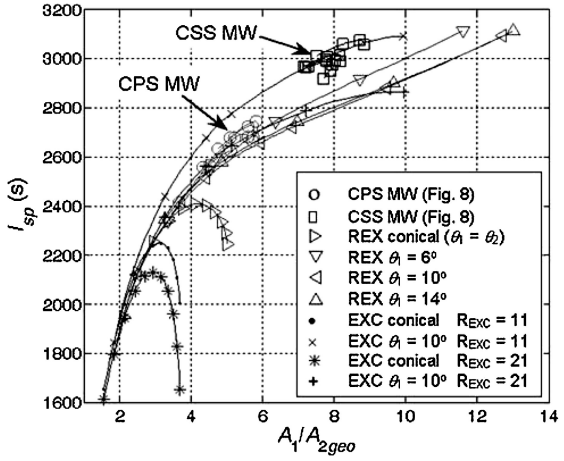

Fig. 9 Comparison of intake designs by calculating engine performance.

before the Mack disk growth becomes significant. It is apparent that there is little difference between the curves, indicating that the relationship is not strongly influenced by N. However, advantages of low N for CPS MW intakes include smaller internal contractions for starting and larger throat hydraulic diameters to minimize isolator and combustion friction.

The full mass capture engine performance of CPS and CSS MW intakes shown in Fig. 8 are compared against axisymmetric reexpansion (REX)[7] intakes and external compression (EXC) intakes in Fig. 9 as a function of total contraction ratio. For all intakes $M_1 = 7.0$, $Re_D = 1.57 \times 10^6$, and $D_\infty = 0.35$ m. For clarity, only the curves for equilibrium nozzle flow are shown; the same trends are apparent but at lower I_{sp} if frozen flow is assumed.

The REX and EXC intakes (Fig. 10) have isentropic-spike or conical compression surfaces that focus all waves onto the cowl lip at full mass capture; the REX intakes have a cowl aligned with the axial direction and an internal contraction that is lower than the Kantrowitz limit by an amount attributed to the boundary-layer displacement thickness; the EXC intakes have a cowl that is initially aligned with the deflected flow, then turns the captured flow to the axial direction gradually in a constant-area duct. Turning losses in the EXC intakes are neglected and cowl wave drag is estimated using the MOC to calculate the external pressure, assuming an external cowl radius of 11 or 21 times the initial duct height. Cowl skin friction is calculated using a laminar flat-plate correlation based on momentum thickness, obtained using the momentum integral method.

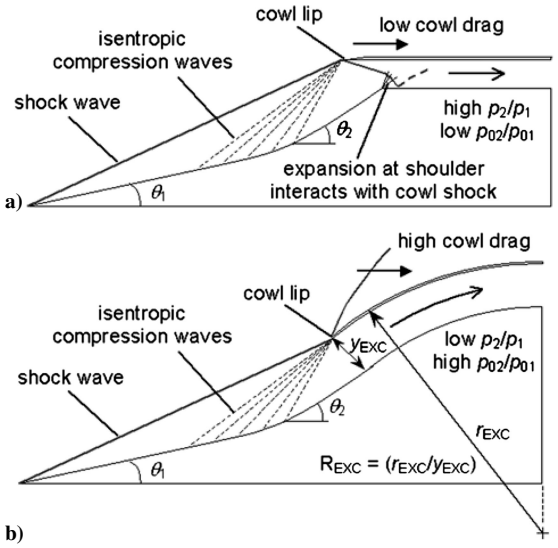

Fig. 10 Schematic diagram of a) REX intake and b) EXC intake.

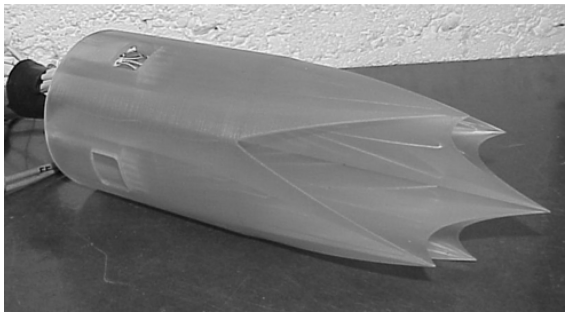

Fig. 11 CPS410 intake model.

For a given contraction ratio, the full mass capture engine performances of the MW intakes and isentropic-spike designs do not differ significantly; specific impulse for these intakes increases with total contraction. Intakes with conical compression surfaces have lower performances and optimum contraction ratios due to increasing wave loss across the conical shock wave with contraction ratio for these intakes. The curves for EXC intakes represent upper limits to their performance as turning losses are neglected. Because of the similarity of full mass capture engine performance of different intake concepts at a given contraction ratio, the criteria for selecting an intake design is most likely to depend on other factors such as intake self-starting ability, the backpressure that can be tolerated, isolator and combustor friction, performance over the flight trajectory, and operation at incidence.

V. Experimental Program

A four-module CPS MW intake model (CPS410) (Fig. 11) was designed for full mass capture at $M_1 = 7.1$, $Re_D = 2.0 \times 10^6$, and $T_w/T_{01} \approx 0.46$. The model was tested at these conditions in the University of Oxford gun tunnel, which produced its flow through a contoured nozzle for 60 ms, attaining constant stagnation pressure for the last 20 ms of the run at a nominal pressure $p_{01} = 6.34$ MPa. A stagnation pressure trace is shown in Fig. 12. The nominal stagnation temperature $T_{01} = 720$ K was calculated from the measured pressure history in the gun tunnel barrel accounting for entropy increase across shocks and applying a 15% reduction to account for the gun barrel heat transfer measured by Buttsworth and Jones.[14]

The inviscid baseline CPS flowfield was designed to have $\theta_{w1} = 10$ deg and $D_\infty = 0.1$ m, but an erroneous boundary-layer correction was applied to the inviscid MW surfaces that underestimated the correct displacement thickness. Consequently, the model's geometric contraction of $A_1/A_{2\text{geo}} = 5.10$, was 13% greater than the

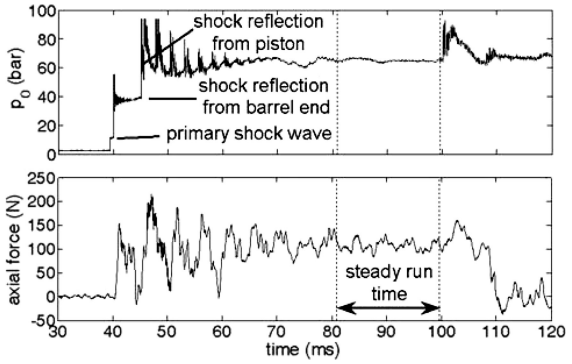

Fig. 12 Gun tunnel stagnation pressure trace and axial force measurement.

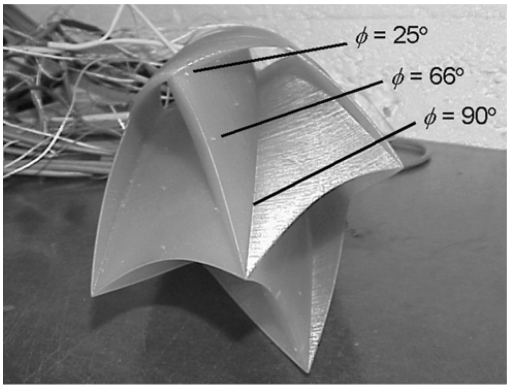

Fig. 13 Pressure taps along streamlines in CPS410 intake model.

geometric contraction ratio of 4.51 calculated using the local-flat-plate momentum integral method. Because the geometric contour does not perfectly conserve the inviscid flowfield, some uncertainty is introduced in determining the geometric area of the cowl closure plane, but this was estimated to give a geometric internal contraction of $A_c/A_{2\text{geo}} \approx 1.54$. The CPS410 intake's limiting internal contraction for starting was estimated to be $(A_c/A_2)_K = 1.53$.

The CPS410 model was constructed using stereolithography and incorporates a network of 1-mm-diam tubing for pressure tappings along the $\phi = 90$, 66, and 25 deg streamlines as shown in Fig. 13, where ϕ is defined in Fig. 2. The V-shaped cowl grows with 6-deg slope from the spikes to a thickness of 1 mm. At the crotch, the cowl becomes cylindrical and grows with a 6-deg slope to a total thickness of 2 mm. The edges of the V-shaped cowl and the crotch are sharp internally and have a 1-mm external radius. The spikes, nose, and leading edges between modules have a 0.25-mm radius. From $x = 232$ mm, the geometric cross-sectional area is held constant for 3.26 hydraulic diameters.

The stream-thrust-averaged flow properties delivered by the intake model were determined by solving the conservation equations for the intake's captured flow control volume using measured values of axial force and mass capture.[7] Heat flux is small in comparison with the total enthalpy of the gun tunnel flow and, therefore, could be calculated with sufficient accuracy for the purpose of determining the stream-thrust-averaged quantities.

A. Axial Force Measurement

The intake model was mounted on a hollow sting fitted with strain gauges. Each gauge was supplied by constant current and the individual gauge voltages were numerically combined such that bending strains canceled to give a linear response to axial force (Fig. 12). The measured force comprised axial components due to cowl drag, preentry drag, isolator drag, and the base pressure force, as shown in Eq. (1), where $F_x = F_p + F_f - F_{\text{add}}$ comprises the axial component of the pressure force and frictional force acting on the

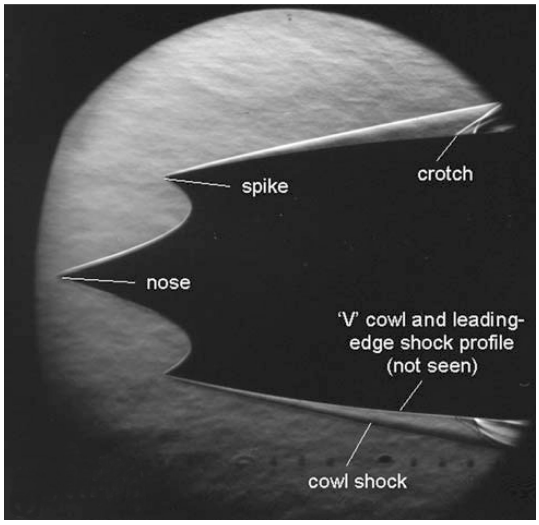

Fig. 14 Schlieren photograph of CPS410 intake at 0-deg incidence, × configuration.

compression surface and the preentry (additive) drag,[7]

$$F_{\mathrm{LC}} = F_x + F_{\mathrm{CD}} + F_{\mathrm{add}} + F_I - F_b \tag{1}$$

Isolator drag was incorporated into intake performance, and $F_x + F_I = 103 \pm 5.3$ N was determined from 1) the measured axial force $F_{\mathrm{LC}} = 108\ \mathrm{N} \pm 2.2\ \mathrm{N}$; 2) cowl drag F_{CD} estimated to be 8.7 N using laminar flat plate values of skin friction and the Rankine–Hugoniot shock wave relations to determine pressure on the 6-deg surfaces; 3) base pressure force F_b not measured but estimated to be $4.0\ \mathrm{N} \pm 4.0\ \mathrm{N}$, assuming $0 < p_b < p_1$; and 4) preentry drag F_{add} assumed zero because of near full mass capture.

B. Mass Flow Measurement

The captured flow was dumped into a plenum attached to the base of the model before being exhausted through six sonic orifices of total area A^* in the plenum base plate. An annular wedge directed the flow from the intake toward the center of the plenum before it passed through a grid intended to produce uniform flow upstream of the choked orifices. Plenum stagnation pressure was measured at two radial locations. Intake mass capture was expressed as

$$\dot{m}_1/\dot{m}_\infty = K_{\dot{m}}\left(A^* \big/ D_\infty^2\right)(P_{0\mathrm{pl}}/p_{01}) \tag{2}$$

with $K_{\dot{m}}$ determined by calibration using two pitot intakes of different D_∞ to provide known capture areas (mass flows). Unfortunately, the calibration intakes produced nonuniform flow in the plenum, and the values of $K_{\dot{m}}$ obtained from the two plenum pressure measurements differed by 3.3%. When these $K_{\dot{m}}$ values are applied to the CPS410 intake, the corresponding mass capture is 0.94 and 1.0. The discrepancy is too large for the measurements to be used in critical analysis.

The schlieren photograph shown in Fig. 14 indeed indicates that the CPS410 mass capture is close to unity because of the following: 1) The leading-edge shock wave cannot be seen along the V-shaped cowl, suggesting that it rests along the edges as designed or lies inside the cowl. 2) The axial location of the crotch shock wave stands ahead of the crotch by approximately 2.0 ± 2.0 mm, hence there is little spilling of flow.

Mass capture for the CPS410 was assumed to be $\dot{m}_1/\dot{m}_\infty = 0.97 \pm 0.03$, which is the average of the preceding values.

VI. Experimental Results

The CPS410 intake was tested in the gun tunnel at incidence up to 8 deg with the modules arranged in the × and + configurations indicated in Fig. 15. All modules started at 4-deg incidence. When tested at 8 deg in the × configuration, only the leeward module unstarted and the other three modules remained started; when tested at 8 deg in the + configuration, the two leeward modules unstarted and the windward modules remained started.

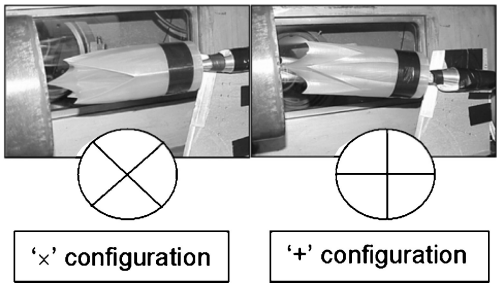

Fig. 15 Test configurations for CPS410 intake model.

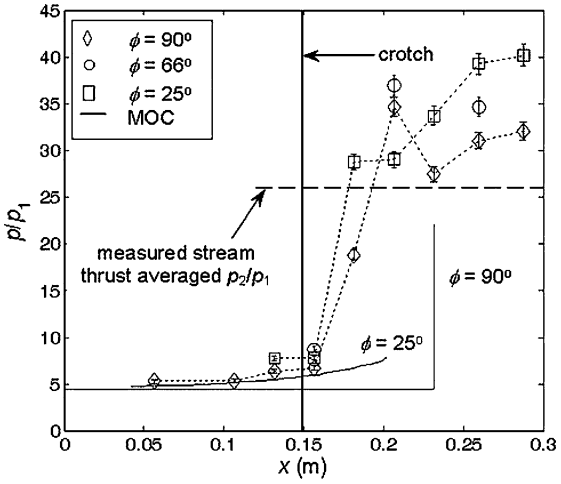

Fig. 16 Measured pressure distribution along CPS410 surface streamlines at 0-deg incidence.

The surface pressure measurements at 0-deg incidence are shown in Fig. 16. Also shown are the calculated pressures along the $\phi = 90$ and 25 deg streamlines for the designed inviscid flowfield. The measured pressures near the start of the $\phi = 90$ deg streamline are slightly higher than calculated, which is an indication of the underestimated correction for displacement thickness. Figure 16 also shows that the swept cowl shock is located farther upstream than calculated by the MOC. This is in part due to terminating the stream tracing methodology at the cowl shock and then enforcing axial surfaces. The measured pressures along the $\phi = 90$ deg streamline are noticeably similar in form to the pressure distribution for a separated shock wave–boundary-layer interaction, shown in Ref. 15. The boundary layer may have separated on the $\phi = 90$ deg streamline in the region of the slight pressure rise at $x = 132$ mm, with the reattachment point upstream of the pressure overshoot at $x = 207$ mm. The pressures at $x = 132$ mm on the $\phi = 25$ deg streamline are also higher than calculated, possibly due to the weak incipient separation shockwaves. The pressure plateaux on the $\phi = 25$ deg streamline around $182 < x < 207$ mm is indicative of a separation bubble, with the pressures subsequently increasing after the reattachment shock. Although the separation on the $\phi = 90$ deg streamline may be upstream of the cowl closure plane, the schlieren image shown in Fig. 14 does not show any separation shockwaves ahead of the crotch, indicating that the separation is contained within the internal part of the intake and does not affect mass capture. The nonuniformity of the CPS410 internal flow is apparent.

The CPS410 model profile was found to be, to a reasonable approximation, geometrically similar to a local-flat-plate boundary-layer-corrected four-module CPS MW intake with inviscid initial angle $\theta_{w1} = 10.7$ deg, and $M_\infty = 7.1$. Figure 17 shows that the calculated pressures for the $\theta_{w1} = 10.7$ deg MW intake are 8% lower than measured along the $\phi = 90$ deg streamline, upstream of the incipient separation.

Table 1 CPS410 measured stream-thrust-averaged flow

Property	Measured value	Calculated value, $F_I = 0$ N and $Q_I/H_{01} = 0$	Calculated value, $F_I \approx 3.2$ N and $Q_I/H_{01} \approx 0.01$
p_2/p_1	26.0 ± 2.2	18	24
T_2/T_1	4.24 ± 0.32	3.1	3.9
M_2/M_1	0.390 ± 0.021	0.50	0.42
$A_1/A_{2\text{geo}}$	5.1	5.1	5.1
η_{KE}	0.900 ± 0.012	0.95	0.93
Q/H_{01}	0.05 ± 0.025	0.02	0.03

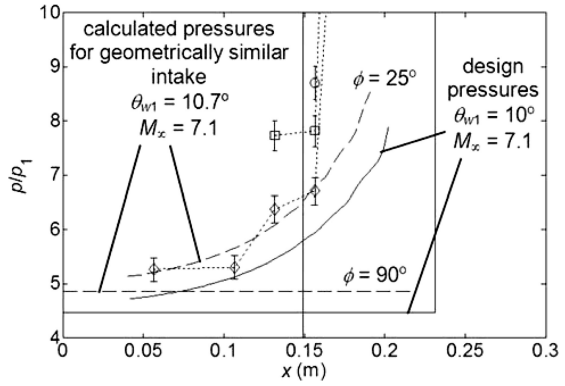

Fig. 17 Comparison with experiment of geometrically similar CPS MW intake with $\theta_{w1} = 10.7$ deg and $M_\infty = 7.1$.

A. Stream-Thrust-Averaged Intake Performance

The CPS410 stream-thrust-averaged properties deduced from the measurements are presented in the second column of Table 1. Intake heat transfer was estimated using fully developed pipe flow theory to model the isolator and the internal contraction. The analysis indicates an isolator skin-friction coefficient $C_{\text{fl}} = F_I/\frac{1}{2}\rho_{2m}v_2^2A_{s1}$ of 0.005 due to the 15-μm stereolithography roughness, using properties evaluated at Eckert's reference temperature. Intake drag and heat transfer upstream of the crotch were estimated using intake stream properties from the MOC. The internal contraction pressure force was set to the value required to make the total drag equal $F_x + F_I$. Wall temperatures were calculated from the corresponding heat flux by treating the model as semi-infinite. An accuracy of 50% was assumed for the heat transfer calculation.

The measured capability (compression) is significantly higher, and the measured efficiency is significantly lower than the calculated values shown in the third column of Table 1. These values were obtained using stream properties from the MOC, assuming attached boundary layers, and neglecting isolator skin friction and heat transfer. The calculated values shown in the last column of Table 1 incorporate approximate values for the internal contraction wave drag, isolator skin friction, and heat transfer, and are closer to the measured values. Wave drag in the internal contraction was estimated to be ~5.3 N by integrating the measured pressures shown in Fig. 16 downstream of the crotch. Isolator skin friction and heat transfer were estimated using fully developed pipe flow theory with $C_{\text{fl}} = 0.005$ and with properties evaluated at Eckert's reference temperature. The pressure force upstream of the crotch and skin friction and heat transfer over the compression surface were estimated using stream properties from the MOC.

B. CPS410 Starting Tests

The starting mechanism of intakes in pulse facilities such as the gun tunnel is different from the quasi-steady starting mechanism of intakes in flight. Nonself-starting intakes can be started in the unsteady processes of the gun tunnel when the initial test section vacuum pressure is sufficiently low. The CPS410 intake was tested in QinetiQ's High Density Tunnel (HDT) to confirm that it was self-starting. The HDT operates as a heated Ludwieg tube with a valve that gradually opens over a period of 30 ms. It has been demonstrated that axisymmetric internal compression intakes do not start in the facility if the contraction ratio is greater than the Kantrowitz limit (see Ref. 16). The HDT nozzle produced conical flow with Mach number variation $6.9 < M_1 < 7.19$ between the intake nose and crotch.

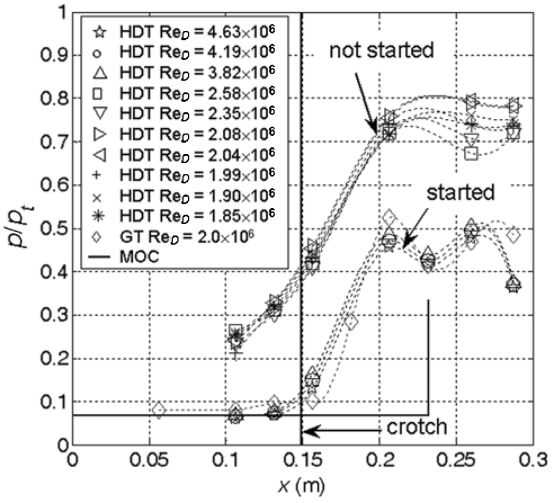

Fig. 18 CPS410 pressure measurements along $\phi = 90$-deg streamline at 0-deg incidence.

The pressure traces in Fig. 18 show that the CPS410 started in the HDT at high Reynolds numbers $3.82 \times 10^6 < Re_D < 4.63 \times 10^6$, but did not start at moderate Reynolds numbers $1.85 \times 10^6 < Re_D < 2.58 \times 10^6$. Even lower Reynolds numbers can be expected in flight. For all tests in the HDT, $T_w/T_{01} \approx 0.7$. These results suggest that the intake will start if the boundary layer is turbulent, but will not start due to separation if the boundary layer remains laminar. The tests demonstrate that it is necessary to incorporate trips to ensure that intake boundary layers are turbulent and, hence more stable against adverse pressure gradients.

VII. Conclusions

The performance of different intake concepts can be compared by evaluating engine performance. The engine cycle accounts for intake capability (compression), efficiency, mass capture, and contribution to vehicle drag. For input to the engine cycle, the stream-thrust-averaged flow produced by intake-isolator designs can be found in wind tunnels by measurement of axial force, mass capture, and heat transfer, knowing the total contraction and freestream properties.

Flow viscosity in the isolator section greatly increases capability and reduces efficiency. The effect can be sufficiently large that the wind-tunnel data are greatly devalued if the model isolator does not replicate nondimensionally the engine isolator. Viscosity also results in a reduced contraction ratio (and lower performance) because the design must account for significant boundary-layer displacement at the intake throat. The dominance of viscous effects on hypersonic intake performance and operability (starting and flow separations) means that the intakes must be tested at flight Reynolds number and T_w/T_{01} and with all boundary-layer management devices such as trips and steps in place.

The calculated full mass capture engine performance of CPS and CSS MW intakes does not differ significantly from that of REX and EXC isentropic-spike designs with the same contraction ratio. This suggests that the arbiter of one design over another will most likely depend on other factors such as self-starting ability, maximum backpressure, isolator and combustor friction, performance over the flight trajectory, and operation at incidence.

Acknowledgment

This work was carried out as part of the Weapon and Platform Effectors Domain of the Ministry of Defence Research Programme.

References

[1]Mölder, S., and Romeskie, J. M., "Modular Hypersonic Inlets with Conical Flow," *Hypersonic Boundary Layers and Flow-Fields*, CP-30, AGARD, 1968, pp. 9.1–9.22.

[2]Billig, F. S., "Supersonic Combustion Ramjet Missile," *Journal of Propulsion and Power*, Vol. 11, No. 6, 1995, pp. 1139–1146.

[3]Smart, M. K., "Design of Three-Dimensional Hypersonic Inlets with Rectangular-to-Elliptical Shape Transition," *Journal of Propulsion and Power*, Vol. 15, No. 3, 1999, pp. 408–416.

[4]Smart, M. K., "Experimental Testing of a Hypersonic Inlet with Rectangular-to-Elliptical Shape Transition," *Journal of Propulsion and Power*, Vol. 17, No. 2, 2001, pp. 276–283.

[5]Smart, M. K., and Trexler, C. A., "Mach 4 Performance of Hypersonic Inlet with Rectangular-to-Elliptical Shape Transition," *Journal of Propulsion and Power*, Vol. 20, No. 2, 2004, pp. 288–293.

[6]Van Wie, D. M., "Scramjet Inlets," *Scramjet Propulsion*, edited by E. T. Curran and S. N. B. Murthy, Progress in Astronautics and Aeronautics, Vol. 189, AIAA, Reston, VA, 2000, Chap. 7, pp. 447–511.

[7]Matthews, A. J., Jones, T. V., and Cain, T. M., "Design and Test of a Hypersonic Isentropic-Spike Intake with Aligned Cowl," *Journal of Propulsion and Power*, Vol. 21, No. 5, 2005, pp. 838–843.

[8]Eckert, E. R. G., "Engineering Relations for Friction and Heat Transfer to Surfaces in High Velocity Flow," *Journal of the Aeronautical Sciences*, Vol. 22, No. 8, 1955, pp. 585–587.

[9]Van Driest, E. R., "The Problem of Aerodynamic Heating," *Aeronautical Engineering Review*, Vol. 15, No. 10, 1956, pp. 26–41.

[10]Stollery, J. L., "Supersonic Turbulent Boundary Layers: Some Comparisons Between Experiment and a Simple Theory," *Aeronautical Quarterly*, Vol. 28, No. 2, 1976, pp. 87–98.

[11]Kantrowitz, A., and Donaldson, C., "Preliminary Investigation of Supersonic Diffusers," NACA WR L-713, May 1945.

[12]McBride, B., and Gordon, S., "NASA-Lewis Chemical Equilibrium Program CEA," NASA RP-1311, Pt. 1, Oct. 1994.

[13]McBride, B., and Gordon, S., "NASA-Lewis Chemical Equilibrium Program CEA," NASA RP-1311, Pt. 2, Oct. 1996.

[14]Buttsworth, D. R., and Jones, T. V., "A Fast-Response Total Temperature Probe for Unsteady Compressible Flows," American Society of Mechanical Engineers, Paper 96-GT-350, June 1996.

[15]Prince, S. A., Vannahme, M., and Stollery, J. L., "Experiments on the Hypersonic Turbulent Shock-Wave/Boundary-Layer Interaction and the Effects of Surface Roughness," *Aeronautical Journal*, Vol. 109, No. 1094, 2005, pp. 177–185.

[16]Zanchetta, M., and Cain, T., "An Axisymmetric Internal Compression Inlet," AIAA Paper 98-1525, April 1998.